NAVORD REPORT 3757

NOL HYPERSONIC TUNNEL NO. 4 RESULTS VI: EXPERIMENTIAL AND THEORETICAL INVESTIGATION OF THE BOUNDARY LAYER AND HEAT TRANSFER CHARACTERISTICS OF A COOLED HYPERSONIC WEDGE NOZZLE AT A MACH NUMBER OF 5.5

8 JULY 1954

U. S. NAVAL ORDNANCE LABORATORY
WHITE OAK, MARYLAND

NOTICE: THIS DOCUMENT CONTAINS INFORMATION AFFECTING T
NATIONAL DEFENSE OF THE UNITED STATES WITHIN THE MEANI
OF THE ESPIONAGE LAWS, TITLE 18, U.S.C., SECTIONS 793 and 794
THE TRANSMISSION OR THE REVELATION OF ITS CONTENTS IN
ANY MANNER TO AN UNAUTHORIZED PERSON IS PROHIBITED BY

NAVORD Report 3757

Aeroballistic Research Report 245

NOL HYPERSONIC TUNNEL NO. 4 RESULTS VI: EXPERIMENTAL AND THEORETICAL INVESTIGATION OF THE BOUNDARY LAYER AND HEAT TRANSFER CHARACTERISTICS OF A COOLED HYPERSONIC WEDGE NOZZLE AT A MACH NUMBER OF 5.5

Prepared by:

E. M. Winkler and Jerome Persh

ABSTRACT: Experimental and theoretical investigations were conducted of the nozzle wall heat transfer and boundary layer transition in the NOL 12 x 12 cm Hypersonic Tunnel No. 4 at a Mach number setting of the wedge nozzle of 5.5 and a constant supply temperature of 430° K. The experimental data consist of local heat transfer and surface probe measurements at several axial locations along the nozzle wall, overall heat transfer measurements, and boundary layer surveys at various supply air pressures. These data provide needed information for the design and construction of hypersonic nozzles. The theoretical studies give a method by which the boundary layer development and heat transfer to the nozzle wall can be computed from properly selected (or measured) initial conditions and the measured position of the transition point along the nozzle wall. The agreement between experimental and theoretical data sufficiently supports the usefulness of the analytical method for design applications.

U. S. NAVAL ORDNANCE LABORATORY
WHITE OAK, MARYLAND

NAVORD Report 3757 8 July 1954

This is the sixth NAVORD Report on investigations carried out in the continuous NOL 12 x 12 cm Hypersonic Tunnel No. 4. The present investigation was carried out to provide detailed information on the heat transfer to the nozzle wall under conditions where transition from a laminar to a turbulent boundary layer occurs in the throat region of the nozzle. The work was jointly sponsored by the U. S. Naval Bureau of Ordnance and the U. S. Air Force, Flight Research Laboratory and was performed under Task NOL-M9a-108-1-54. The authors are indebted to Dr. R. K. Lobb for many stimulating discussions during the course of the investigation. The cooperation of Messrs. L. L. Liccini and R. Garren, who participated in the tests, is acknowledged.

JOHN T. HAYWARD
Captain, USN
Commander

H. H. KURZWEG, Chief
Aeroballistic Research Department
By direction

CONTENTS

	Page
Introduction	1
Equipment and Experimental Techniques	1
Results	2
Theoretical Calculations and Comparison with Experiments	4
Summary	9
References	10

ILLUSTRATIONS

		Page
Figure 1.	Boundary layer transition along nozzle wall as function of supply pressure	11
Figure 2.	Overall heat transfer to one nozzle block as function of supply pressure	12
Figure 3.	Boundary layer velocity profiles near nozzle exit for three values of the supply pressure	13
Figure 4.	Boundary layer temperature profiles near nozzle exit for three values of the supply pressure	14
Figure 5.	Variation of the skin friction coefficient with supply pressure for four axial locations along the nozzle wall	15
Figure 6.	Variation of $\left[\frac{\gamma + 2 - M_\infty^2}{1 + \frac{\gamma-1}{2} M_\infty^2}\right] \frac{1}{M_\infty} \frac{dM_\infty}{dx}$ with axial distance along nozzle	16
Figure 7.	Variation of momentum thickness with axial distance along nozzle	17
Figure 8.	Variation of skin friction coefficient with axial distance along nozzle	18
Figure 9.	Comparison between experimental and theoretical boundary layer profiles	
	a. for a supply pressure of 1 atmosphere	19
	b. for a supply pressure of 4 atmospheres	20
	c. for a supply pressure of 8 atmospheres	21
Figure 10.	Variation of the wall temperature with axial distance along nozzle for three values of the supply pressure	22
Figure 11.	Variation of throat Reynolds number based on momentum thickness with supply pressure	23

SYMBOLS

A_w nozzle surface area per coolant tube

c_f local skin friction coefficient based on free-stream conditions $\frac{\tau}{1/2\,\rho_\infty u_\infty^2}$

C constant for laminar skin friction law

c_p specific heat at constant pressure

f(x) pressure gradient term for momentum equation

$$\frac{1}{M_\infty}\frac{dM_\infty}{dx}\left[\frac{H+2-M_\infty^2}{1+\frac{\gamma-1}{2}M_\infty^2}\right]$$

f_1 (M) Mach number function for laminar skin friction law

$$\frac{1}{\left(1+\frac{\gamma-1}{2}M_\infty^2\right)^{.091}}$$

f_2 (M) Mach number function for turbulent skin friction law

$$\frac{1}{\left(1+\frac{\gamma-1}{2}M_\infty^2\right)^{.42}}$$

h_a local heat transfer coefficient for air

H boundary layer shape parameter defined as δ^*/θ

k thermal conductivity

L wetted nozzle length

M Mach number

Pr Prandtl number

p_o stagnation pressure

p_o' pitot pressure

p static pressure

q local heat transfer rate

Q overall heat transfer rate

Re Reynolds number based on free-stream conditions

r	recovery factor
St	Stanton number
T	local static temperature
T_e	equilibrium temperature for zero heat transfer
T_w	local wall temperature
T_b	coolant tube surface temperature
T_c	coolant temperature
u	velocity
W_c	weight flow rate of coolant
x	longitudinal distance along nozzle axis
y	distance perpendicular to wall
γ	ratio of specific heats
δ	total boundary layer thickness
δ^*	displacement thickness $\int_0^\delta \left(1 - \frac{\rho u}{\rho_\infty u_\infty}\right) dy$
θ	momentum thickness $\int_0^\delta \frac{\rho u}{\rho_\infty u_\infty} \left[1 - \frac{u}{u_\infty}\right] dy$
μ	viscosity
ρ	density
τ	shear stress

Subscripts

w	values based on wall conditions
θ	values based on momentum thickness
∞	values based on free-stream condition outside the boundary layer

NOL HYPERSONIC TUNNEL NO. 4 RESULTS VI: EXPERIMENTAL AND THEORETICAL INVESTIGATION OF THE BOUNDARY LAYER AND HEAT TRANSFER CHARACTERISTICS OF A COOLED HYPERSONIC WEDGE NOZZLE AT A MACH NUMBER OF 5.5

INTRODUCTION

1. For the design of hypersonic wind tunnels intended to operate at very high supply pressures and temperatures, in the order of 50 to 100 atmospheres and 1,000° K respectively, information on the local heat transfer to the nozzle throat and overall heat transfer to the entire nozzle block are needed to pose safe construction criteria.

2. In contrast to the large amount of theoretical work done on the solution of the hypersonic heat transfer and skin friction problems, relatively few experimental investigations have been performed. The comparison between the available data and theories shows certain, though moderate, disagreements in the trend as well as in the absolute value of parameters obtained theoretically which makes an accurate prediction of heat transfer and skin friction data beyond the range of available experimental data difficult.

3. In a previous NAVORD, experimental and theoretical investigations of a cooled hypersonic wedge nozzle were reported (reference 1). The purpose of the present investigation is to furnish more detailed information regarding the heat transfer and boundary layer characteristics of the NOL hypersonic wind tunnel, and also to indicate methods by which such data may be calculated.

Equipment and Experimental Techniques

4. All measurements were made in the NOL 12 x 12 cm Hypersonic Wind Tunnel No. 4 (reference 1). A Mach number 5.5 setting* of the nozzle was selected for these tests since with this setting and the present operational range of the wind tunnel,

---

* The terminology "Mach number 5.5 setting" is used only to define the nozzle geometry. The actual free-stream Mach number obtained at the survey station is about 5.0.

the desired test conditions could be accomplished, namely that transition from a laminar to a turbulent nozzle wall boundary layer occurs close to the nozzle throat, and also that the physical dimensions of the throat height are roughly comparable to those of larger hypersonic wind tunnels to be built in this country.

5. The supply air temperature was kept constant at 430° K for all tests. The supply pressure was varied from about 1 to 15 atmospheres. A steady-state nozzle wall temperature distribution was maintained by a coolant flow rate of 3 gallons per minute per nozzle block.

6. Local values of heat transfer and nozzle surface temperatures were determined at four stations along the centerline of one nozzle block ($x = -.397$, $+2.14$, 3.42, and 50 cm, where $x = 0$ is the position of the throat). These results are deduced from the known heat conductivity of the nozzle material and temperature measurements made with four thermocouples imbedded at each station in the nozzle wall at various distances from the surface (reference 1). The overall heat transfer to one nozzle block is obtained by measuring the coolant flow rate, the temperature of the incoming water, and the temperature rise of the water. Depending upon the supply pressure, practically steady-state conditions were reached for all measurements after 5 to 10 minutes operation. The accuracy of the absolute temperature readings is ±.2° C; the temperature differences were read to ±.01° C.

7. Surface pitot probes were used in conjunction with free-stream static pressure probes at a number of axial stations along the nozzle wall ($x = 2.54$, 5.08, 15.25, 22.85, and 50 cm) to determine the beginning and end of transition as a function of the supply pressure.

8. The boundary layer was surveyed at the center of the nozzle wall at the 50 cm station for supply pressures of 1, 4, and 8 atmospheres. For each survey, pitot and static pressures, stagnation and wall temperatures, and the wall temperature gradient perpendicular to the nozzle surface were recorded (references 2 and 3). The accuracy of the pressure readings is ± .1 mm Hg for pressures above 20 mm Hg and ± 1 micron for pressures below 20 mm Hg. The latter measurements were made with a precision oil manometer. The stagnation temperatures are measured to ±.2° C.

RESULTS

9. The mapping of the transition region along the length of the nozzle is accomplished by using both the local heat transfer data and the surface probe measurements. By plotting the

ratios p_o'/p and the wall temperature gradient $\Delta T/\Delta y$ as functions of the supply pressure, curves of the type shown below are obtained for each station.

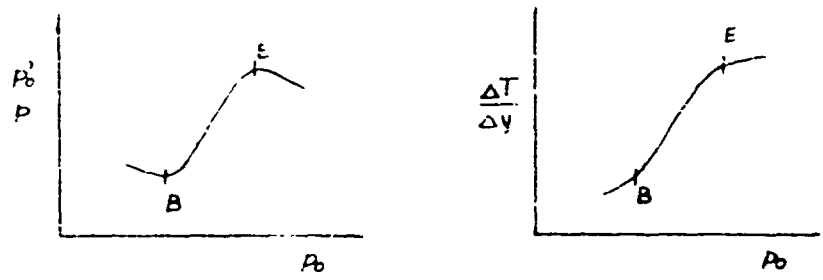

Transition is assumed to begin at the point indicated as B and to end at E. The supply pressures corresponding to the points B and E are then plotted as a function of the axial distance along the nozzle surface (Figure 1). The points for the onset of transition at $x = -.397$ and $x = +2.14$ are not connected as part of the curve because of the uncertainties in the throat region. A connection of these points would indicate the lower limit for the onset of transition ahead of the throat. It is conceivable that completely turbulent flow does not exist at the throat due to the large pressure gradient and heat removal at this point.

10. The overall heat transfer (Q) to the nozzle block was calculated from the temperature increase of the coolant water and the weighted water flow rate using the following relation

$$Q = W_c c_p \Delta T$$

The results of these calculations are shown as a function of the supply pressure in Figure 2. This curve indicates that for pressures up to 4.4 atmospheres the overall heat transfer corresponds to principally laminar flow conditions over the nozzle length, and beyond 6.4 atmospheres it may be assumed to correspond to principally turbulent flow over the nozzle length. The pressures at the end of the laminar region and at the beginning of the turbulent region are in agreement with the pressures for the onset of transition at $x = 2.14$ and $x = -.397$, respectively (see Figure 1). From this comparison we may conclude that for pressures larger than 6.4 atmospheres the axial extent of the laminar region at the throat is narrow (or non-existent) so that the overall heat transfer indicates turbulent flow along the entire length of the nozzle.

11. Boundary layer velocity and temperature profiles at the 50 cm station were evaluated from measured pressure and temperature data as described in reference 2. Laminar profiles were measured for 1 atmosphere supply pressure and turbulent profiles for 4 and 8 atmospheres, Figures 3 and 4, in accordance with the results shown in Figure 1.

12. Values of local skin friction were determined at four stations along the nozzle wall from measured wall temperatures and wall temperature gradients using a modified Reynolds analogy

$$C_f = 2\,St_\infty\,\rho_r^{\,2/3} \qquad (1)$$

where by definition

$$St_\infty = \frac{K\,(\Delta T/\Delta y)}{(T_e - T_w)\,C_p\,u_\infty\,\rho_\infty} \qquad (2)$$

u_∞ and ρ_∞ were evaluated from temperature and pressure measured at these locations. The equilibrium wall temperature T_e was calculated using $r = Pr^{1/3}$ for turbulent flow and $r = Pr^{\frac{1}{2}}$ for laminar flow and $Pr = .72$. The variation of c_f with supply pressure is shown in Figure 5 for the four measured points. The agreement between [illegible] dicated beginning and end of transition on these curves and those obtained by the surface probe is in all cases good. This can be deduced from the results shown in Figure 1.

Theoretical Calculations and Comparison with Experiments

13. The theoretical calculations are concerned with (a) a prediction of the boundary layer development along the nozzle wall, and (b) a determination of the local and overall heat transfer. The present analysis is a refinement of the method discussed in reference 1; however, the fundamental formulation is similar. The utility of the method resulting from this analysis is then illustrated by comparison with the experimental data. In general, the accuracy of numerical results is found essentially dependent on a knowledge of the axial location of the transition point along the nozzle wall. For the present results, the experimentally determined transition points were used.

14. The boundary layer momentum thickness development is calculated by a step-wise solution of the momentum integral equation (reference 4)

$$\frac{d\theta}{dx} = \frac{c_f}{2} - \theta\left[\frac{1}{M_\infty}\,\frac{dM_\infty}{dx}\left(\frac{H + 2 - M_\infty^{\,2}}{1 + \frac{\gamma - 1}{2} M_\infty^{\,2}}\right)\right] \qquad (3)$$

Assuming that the velocity distribution as determined by one-dimensional flow considerations is sufficiently accurate for all subsequent boundary layer calculations, the bracketed term of equation (3) can be evaluated once the shape parameter is known. For laminar flow throughout the nozzle, H was calculated from (reference 4)

$$H = 2.59 \left[1 + .277 M_\infty^2 \right] \qquad (4)$$

and for completely turbulent flow the tabulated data of reference 5 were used for a power profile exponent of 1/7. These values of H refer to the case of zero heat transfer. As will be shown later, the overall results are not sensitive, except for marginal cases, to the assumed H values for the range of heat transfer conditions at which the experiments were made. Figure 6 shows the bracketed term for wholly laminar and wholly turbulent flow as a function of the distance along the nozzle axis. Using the experimentally determined transition points, the course of the bracketed term for any supply pressure can be traced. In the transition region, a faired line connects the laminar and turbulent curves of Figure 6.

15. Equation (3) can be written in a simpler form

$$\frac{d\theta}{dx} = \frac{c_f}{2} - \theta f(x) \qquad (5)$$

with $f(x)$ replacing the bracketed term. Before equation (5) can be solved in a step-wise manner from known conditions at a given starting point, a method for calculating c_f values must be given.

16. The following skin friction formulas were used

$$\text{Laminar flow region} \qquad c_f = \frac{C}{Re_\theta} f_1(M) \qquad (6)$$

$$\text{Turbulent flow region} \qquad c_f = \frac{.033}{Re_\theta^{.268}} f_2(M) \qquad (7)$$

where C is a constant which is dependent on $Re_\theta \frac{\theta}{u_\infty} \frac{du_\infty}{dx}$, and for $f_1(M)$ and $f_2(M)$ the following relations were used which represent an empirical fit to the available experimental results.

$$f_1(M) = \frac{1}{\left(1 + \frac{\gamma-1}{2} M_\infty^2\right)^{.091}} \qquad (8)$$

$$f_2(M) = \frac{1}{\left(1 + \frac{\gamma-1}{2} M_\infty^2\right)^{.42}} \qquad (9)$$

The use of the skin friction equations (6) and (7) implies that the skin friction values are unaffected by heat transfer, which is a necessary assumption, since the wall temperatures are indirectly calculated from the boundary layer results and are therefore not available for this step of the procedure. The pressure gradient dependence of the skin friction values, expressed by equation (5), is recognized for the laminar flow region but not for the turbulent flow region. Referring back to equation (4), this seems to be an inconsistency since for the shape parameter the pressure gradient dependence was ignored. However, comparative calculations, with the effect of pressure gradient and heat transfer on the H value included, gave little change in the overall results, due to the fact that values of H become important only in the downstream regions of the nozzle where the pressure gradient term is smaller than the skin friction term of equation (3).

17. In order to determine how precise a set of initial conditions has to be known to yield results of acceptable accuracy, two largely different initial conditions were assumed. One assumption considered the initial boundary layer thickness as almost zero, and the second considered the boundary layer thickness to be one-half the height of the subsonic inlet section. The overall results obtained from either of these assumptions are for all practical purposes the same. This is because of the very steep pressure gradient in the throat region which dominates the values computed from equation (5), regardless of the assumed starting point conditions. The same conclusion regarding the effect of the assumed initial conditions was reached in reference 1.

18. For convenience, the calculations presented in the following are based on experimentally determined c_f values at the $x = -.397$ cm station. A station upstream of the throat was

chosen as the starting point for the calculations because the greatest contribution to the overall heat transfer integral occurs in this region.

19. Comparisons between the calculated results and the available experimental data are shown in Figures 7 through 11 for supply pressures of 1, 4, and 8 atmospheres. Figure 7 shows the variation of the calculated momentum thickness θ with axial distance.

20. Since equation (3) makes no provision for the energy lost due to heat transfer, it is anticipated that the values of momentum thickness calculated from equation (3) are somewhat less than the experimental values. This is due to the increased density near the wall resulting from the large heat transfer along the nozzle, which is not recognized in the theoretical method. (By the same reasoning, the theoretical value of will be somewhat larger than the experimental values.) This is shown by the comparisons in Figure 7.

21. The agreement between the calculated and experimental values of the skin friction, c_f, Figure 8, is within 50 percent at the boundary layer survey station at $x = 50$ cm. Downstream of the throat the deviation is larger, probably due to some inadequacy in determining the skin friction values from the heat transfer measurements in this region of strong pressure gradients. The predicted and experimental velocity and temperature profiles at the 50 cm station are given in Figure 9 (a, b, and c). The laminar profiles, for 1 atmosphere supply pressure, were calculated using the method of reference 6; the turbulent profiles have been calculated using the physical model described in reference 7.

22. As was stated previously, a strong energy removal occurs near the nozzle throat due to the large heat transfer in the region. The comparisons shown in Figure 9 indicate that this energy loss is predominately reflected in the temperature profile and only slightly in the velocity profiles. The wall temperature values for these computations were obtained from the heat transfer calculations described in the following section.

23. The heat transfer calculations were carried out according to the analysis described in detail in reference 1. For convenience, the pertinent equations are listed below:

For the heat transfer from the air to the nozzle wall

$$q = h_a A_w (T_r - T_w) \tag{11}$$

For the heat conduction in the nozzle wall

$$q = .825 A_w (T_w - T_b) \tag{12}$$

For the heat transfer to the cooling water

$$q = 10\, W_c^{.8}\, A_w\, (T_b - T_c) \qquad (13)$$

For the overall heat transfer to the nozzle

$$Q = \frac{A_w}{L} \int_0^L h_a\, (T_e - T_w)\, dx \qquad (14)$$

Values of h_a used in equations (11) and (14) were obtained from the skin friction results of the boundary layer calculations, Reynolds analogy (equation (1)) and

$$h_a = St_\infty \rho_\infty u_\infty c_p \qquad (15)$$

24. The calculations were made for a number of supply pressures. Figure 10 gives a comparison between the calculated and experimental wall temperatures along the nozzle for three different supply pressures. The agreement between both sets of data is within 3 percent over most of the nozzle length. Because the cooling water temperature principally effects the experimental wall temperature, and is a determining factor in the solution of equations (13) through (15), it is apparent that good agreement between experimental and theoretical values of T_w is to be expected. Figure 2 compares the experimental and theoretical data for the overall heat transfer. Although the trend of the experimental Q-values is closely followed by the calculated values, the latter are always slightly smaller than the experimental data. This appears to be inconsistent with the previous results shown in Figure 8, since from the direct proportionality between c_f and h_a, it would be anticipated that the theoretical values of Q should be larger than the experimental values. However, it is reasonable to assume that at the throat, where most of the heat transfer occurs, the theory predicts too low values of c_f. The agreement is, however, within the accuracy that can be ascribed to the calculated data (on the basis of the assumptions underlying the analysis) and to the experimental data.

25. Using some of the theoretical results obtained from the foregoing analysis, additional information was obtained concerning the boundary layer transition at the throat. The

theoretical results indicate that the value of Re_θ calculated for the nominal point of transition remains almost constant at about 400 for all values of supply pressure. This observation implies that the curve describing the onset of transition, Figure 1, may be regarded as a line of Re_θ = const = 400. To determine whether or not a Re_θ value of 400 is or can be exceeded at the nozzle throat, the calculated Re_θ values for $x = 0$ are plotted against supply pressure in Figure 11. It is apparent from this figure that, for the range of supply pressures covered, transition probably does not occur at the throat, assuming that the Reynolds number for the start of transition is the same at the throat as at all points along the length of the nozzle. Furthermore, Re_θ may be greater than 400 since a large amount of heat is removed from the boundary layer at $x = 0$, which has a stabilizing effect on the laminar boundary layer. Such stabilization is accompanied by an increase in the Reynolds number for the start of transition.

SUMMARY

26. Characteristics of the boundary layer and heat transfer to the nozzle wall of the NOL Hypersonic Tunnel No. 4 were determined experimentally and by an analytical method which utilizes known positions of the transition point along the nozzle wall.

27. It was found that the overall results of the calculations are not sensitive to the initial conditions selected.

28. The results of the investigation may be briefly summarized as follows:

a. The location of the transition point along the nozzle wall has been determined by using both heat transfer and surface probe measurements. The agreement between both sets of data is within the experimental accuracy. These results have been checked by observing experimentally the shapes of the boundary layer profiles near the nozzle exit.

b. Local heat transfer to the nozzle wall has been measured at several points along the surface by using imbedded thermocouples. The overall heat transfer to the nozzle wall has also been measured by the overall temperature rise of a known amount of coolant flow. These measurements have been made over a supply pressure range from about 1 to 15 atmospheres.

c. Good agreement between the calculated and experimental overall heat transfer has been found for supply pressures above 4 atmospheres.

d. The results of experimental and theoretical calculations indicate that there is some doubt as to whether turbulent flow ever exists at the nozzle throat.

REFERENCES

1. Wegener, P.; Lobb, R. K.; Winkler, E. M.; Sibulkin, M.; and Staab, H., "NOL Hypersonic Tunnel No. 4 Results V: Experimental and Theoretical Investigation of a Cooled Hypersonic Wedge Nozzle," NAVORD Report 2701, April 1953

2. Lobb, R. K.; Winkler, E. M.; and Persh, Jerome, "Experimental Investigation of Turbulent Boundary Layers in Hypersonic Flow," presented at the 22nd Annual Meeting of the Institute of the Aeronautical Sciences, January 1954, Preprint 452

3. Winkler, E. M., "Design and Calibration of Stagnation Temperature Probes for Use at High Supersonic Speeds and Elevated Temperatures," J. Applied Phys., 25, 231 (1954)

4. Goldstein, S., "Modern Developments in Fluid Dynamics, High Speed Flow," Vols. I and II, L. Howarth, ed., The Clarendon Press (Oxford) 1953

5. Tucker, M., "Approximate Calculation of Turbulent Boundary Layer Development in Compressible Flow," NACA TN 2337, April 1951

6. Monaghan, R. J., "An Approximate Solution of the Compressible Laminar Boundary Layer on a Flat Plate," RAE Tech. Note Aero. 2025 Sup. 96, 1949

7. Donaldson, C. du P., "Skin Friction and Heat Transfer Through Turbulent Boundary Layers for Incompressible Flows," presented at the Heat Transfer and Fluid Mechanics Institute Meeting in Los Angeles, June 1952

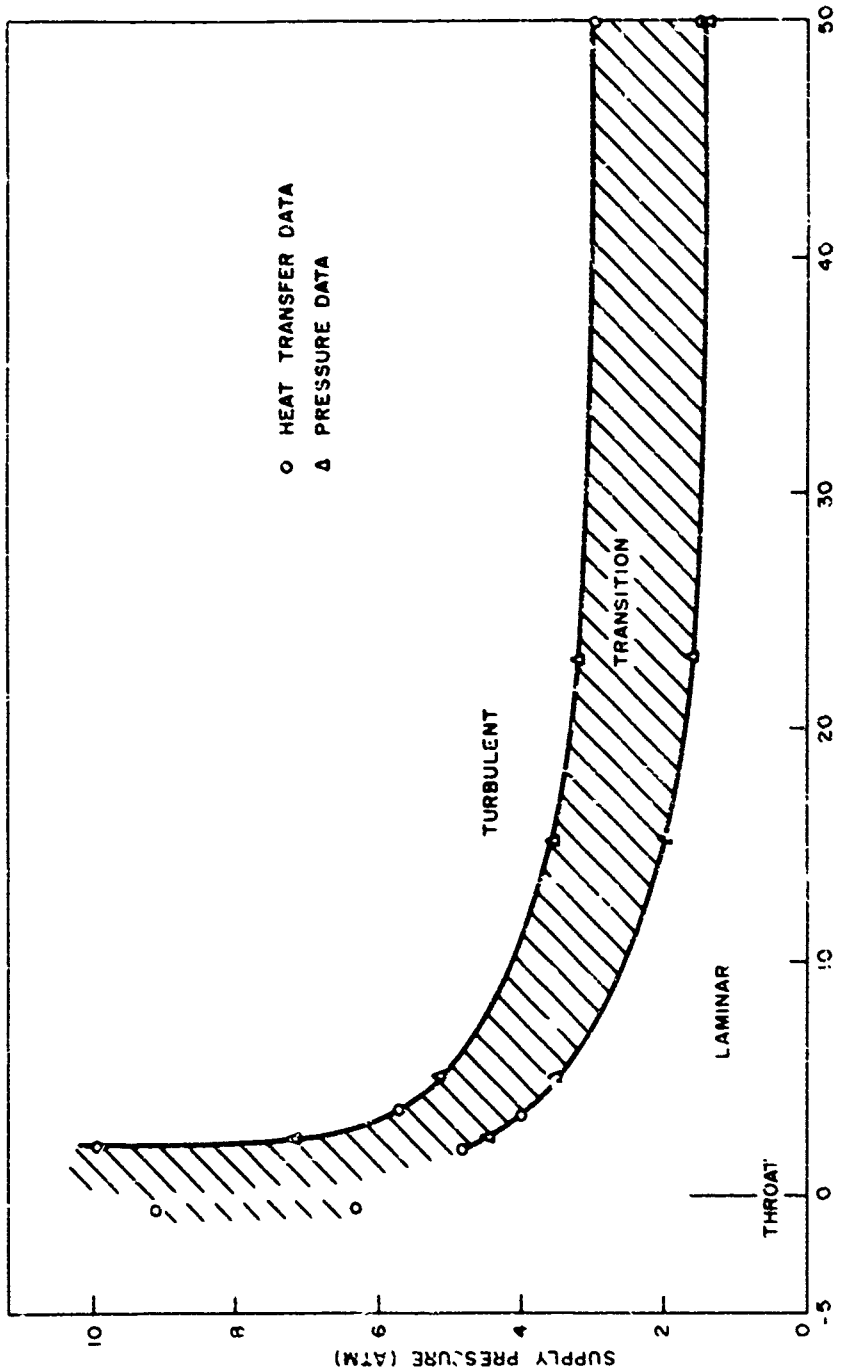

FIG. 1 BOUNDARY LAYER TRANSITION ALONG NOZZLE WALL AS FUNCTION OF SUPPLY PRESSURE

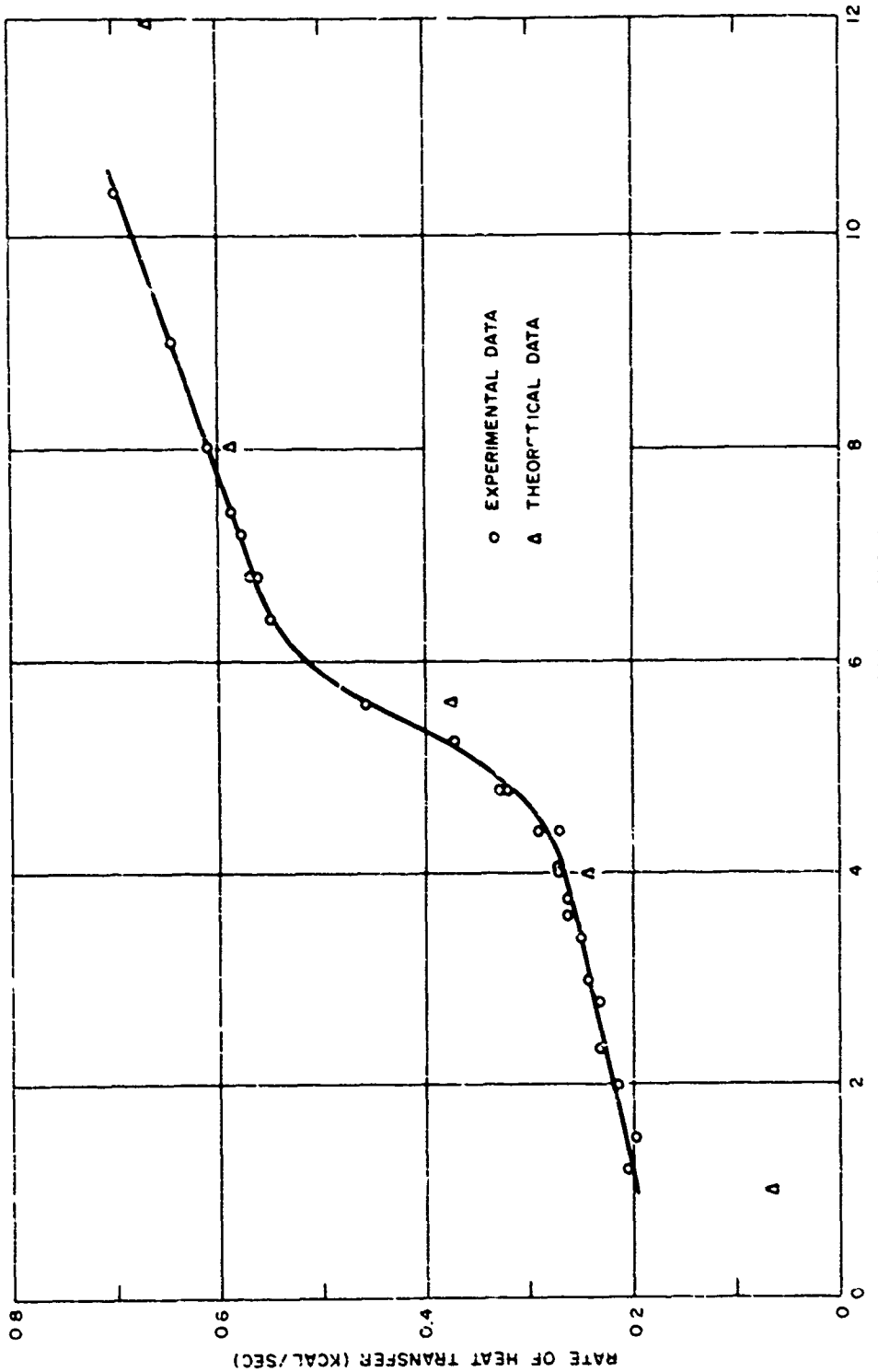

FIG. 2 OVERALL HEAT TRANSFER TO ONE NOZZLE BLOCK AS FUNCTION OF SUPPLY PRESSURE

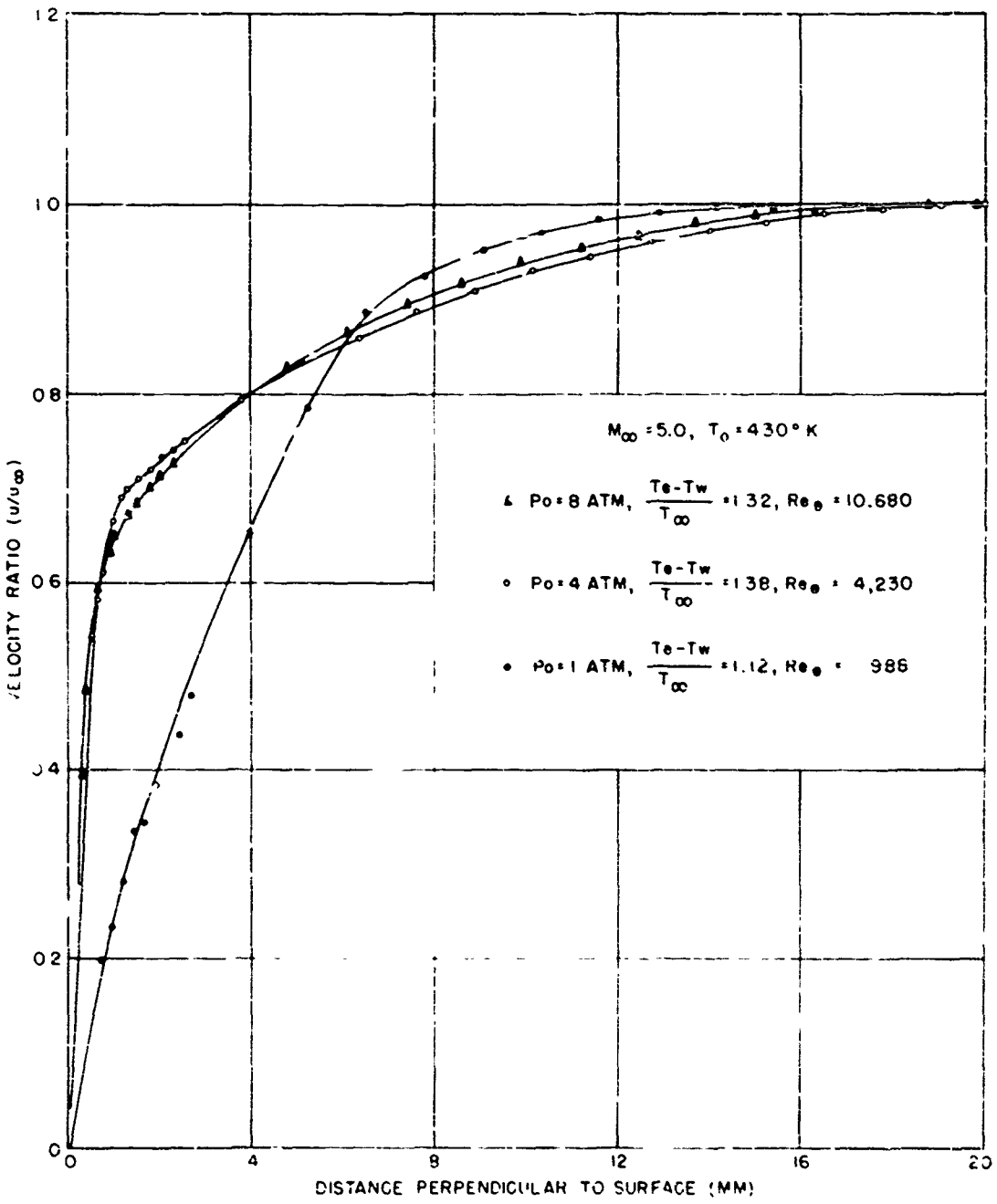

FIG. 3 BOUNDARY LAYER VELOCITY PROFILES NEAR NOZZLE EXIT FOR THREE VALUES OF THE SUPPLY PRESSURE

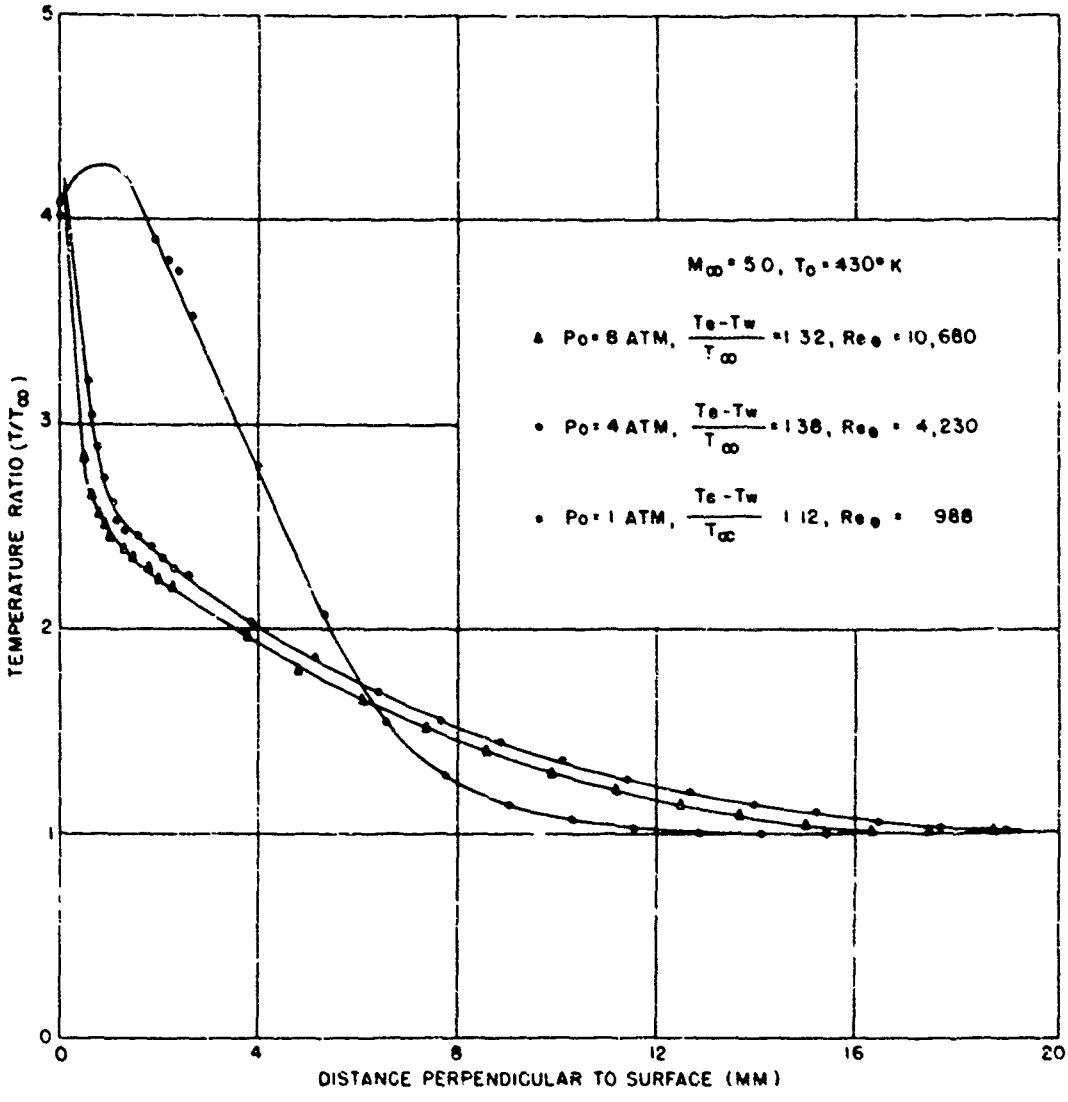

FIG. 4 BOUNDARY LAYER TEMPERATURE PROFILES NEAR NOZZLE EXIT FOR THREE VALUES OF THE SUPPLY PRESSURE

SLOPE NEAR WALL DETERMINED FROM HEAT TRANSFER MEASUREMENT

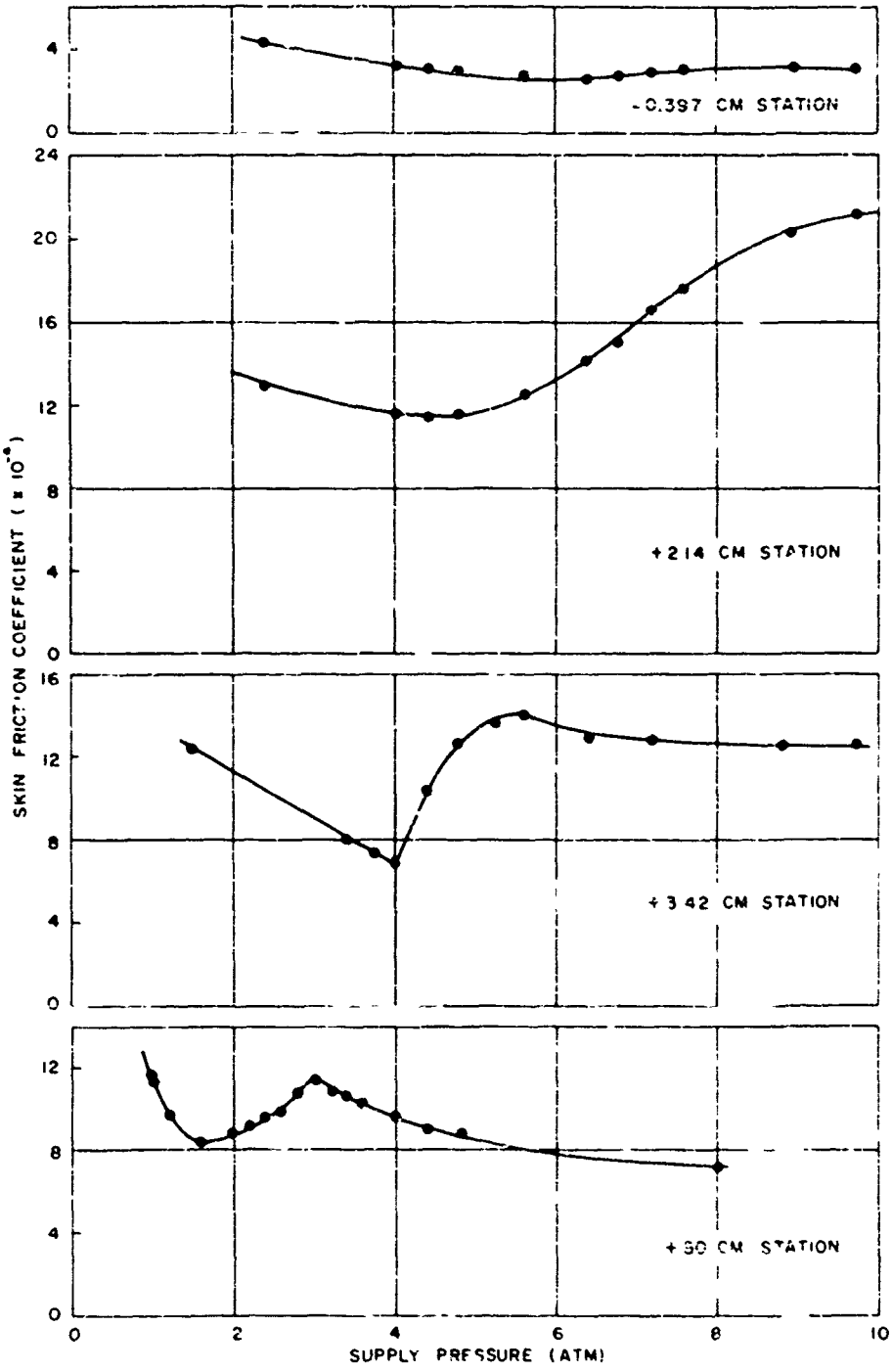

FIG 5

VARIATION OF THE SKIN FRICTION COEFFICIENT WITH SUPPLY PRESSURE FOR FOUR AXIAL LOCATIONS ALONG THE NOZZLE

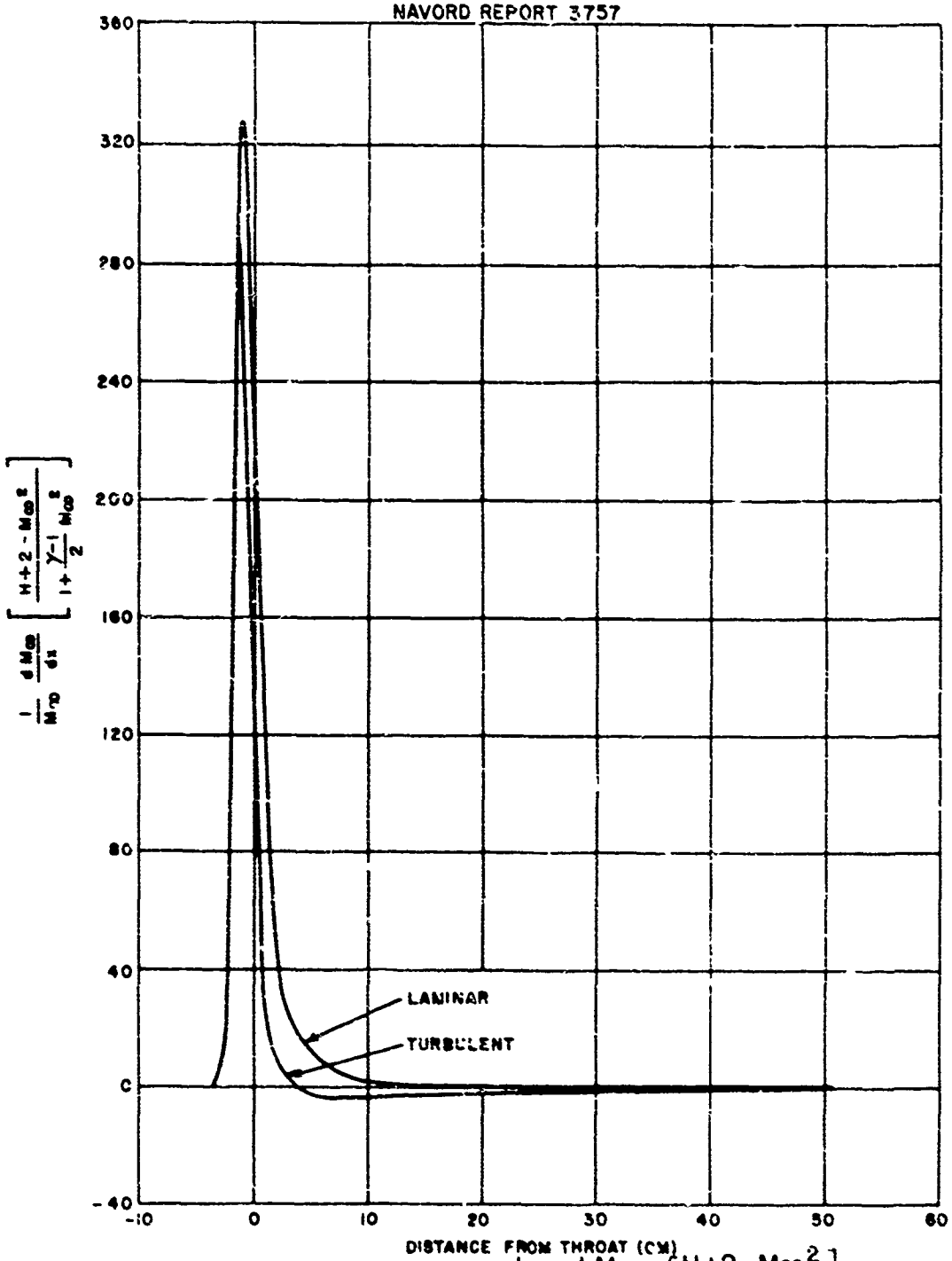

FIG.6 VARIATION OF $\frac{1}{M\infty}\frac{d\,M\infty}{d\,x}\left[\frac{H+2-M\infty^2}{1+\frac{\gamma-1}{2}M\infty^2}\right]$

WITH DISTANCE ALONG NOZZLE

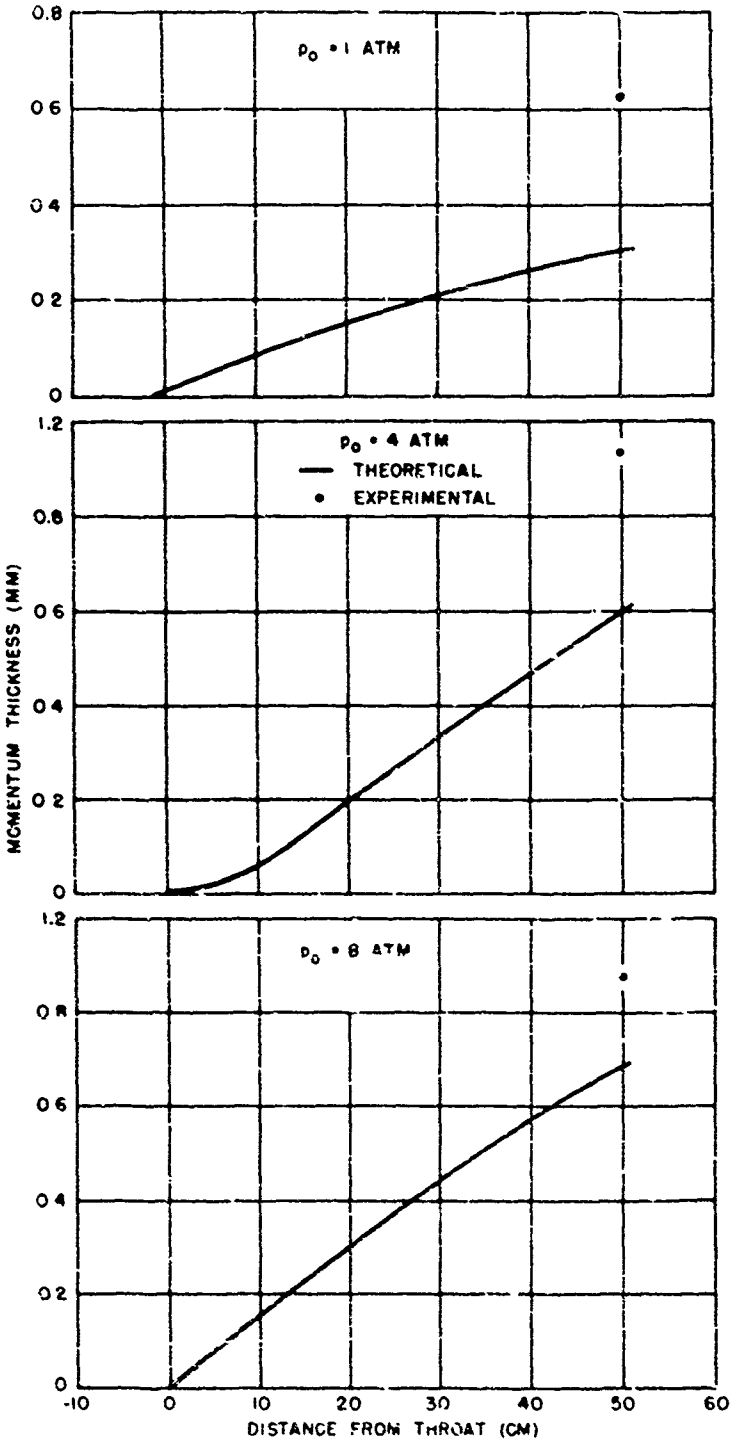

FIG. 7 VARIATION OF MOMENTUM THICKNESS WITH AXIAL DISTANCE ALONG NOZZLE

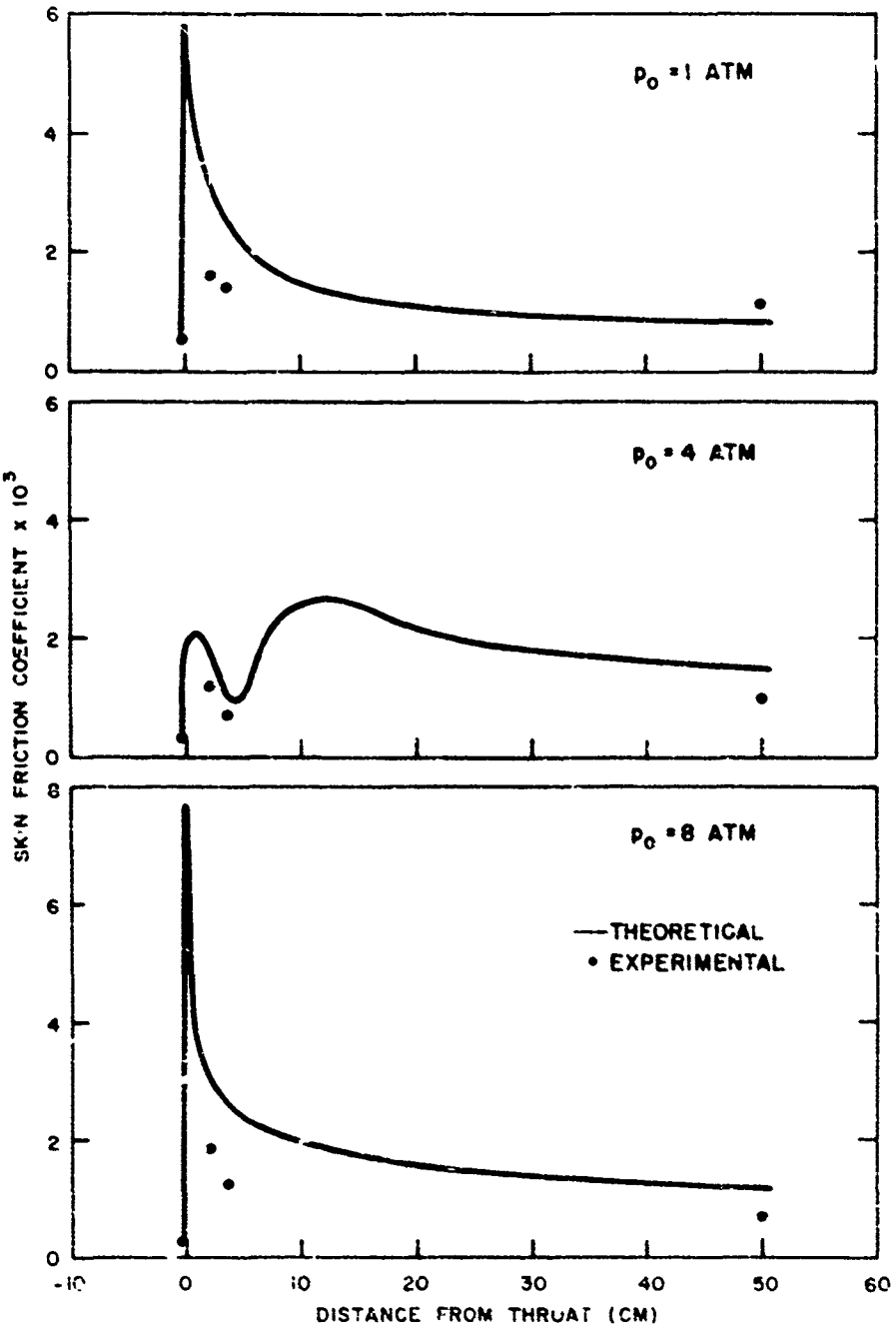

FIG. 8 VARIATION OF SKIN FRICTION COEFFICIENT WITH AXIAL DISTANCE ALONG NOZZLE

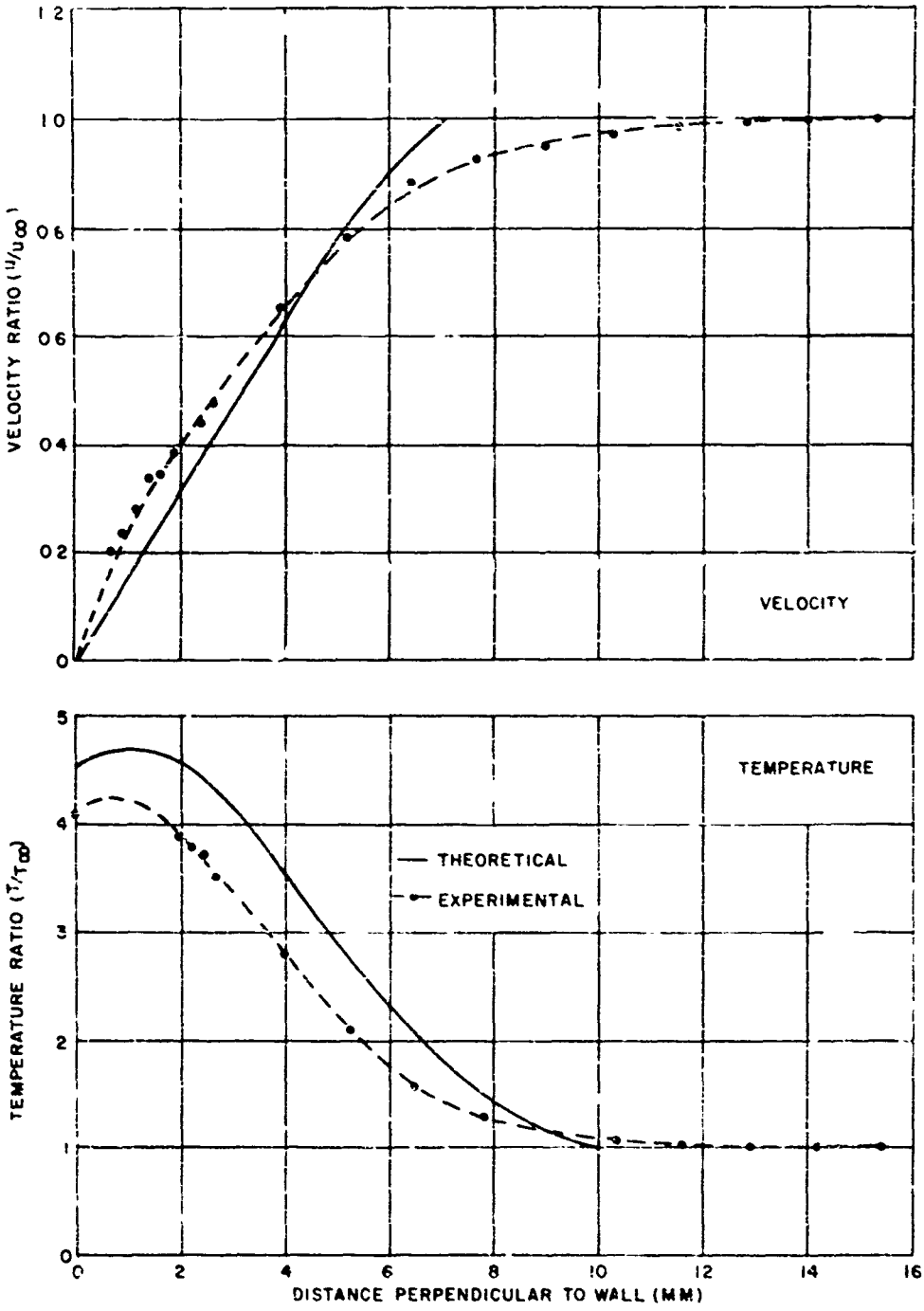

FIG. 9A COMPARISON BETWEEN THEORETICAL AND EXPERIMENTAL LAMINAR BOUNDARY LAYER PROFILES

M_∞ - 5.0 , P_0 = 1 ATM , T_0 = 430°C

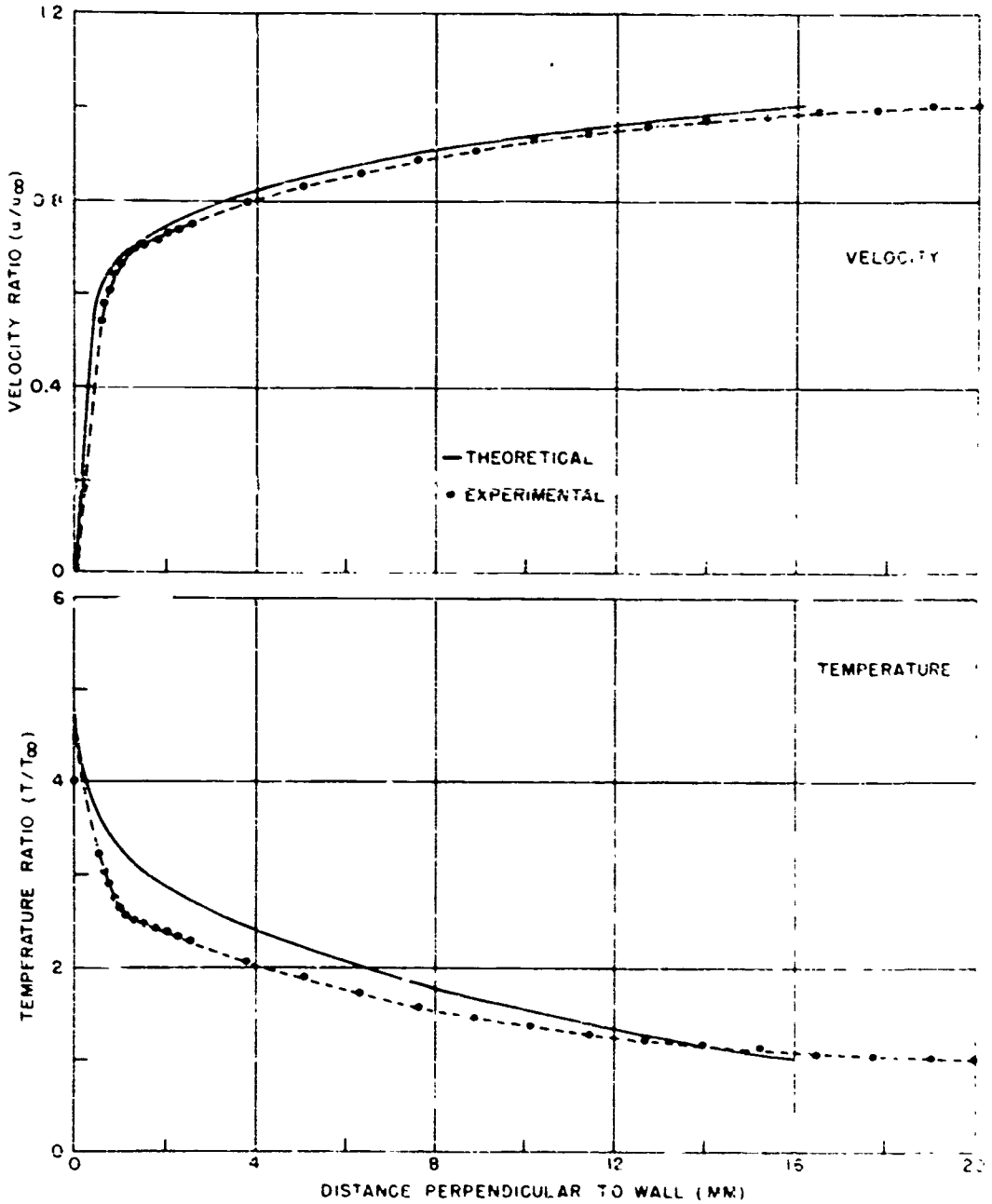

FIG 98 COMPARISON BETWEEN THEORETICAL AND EXPERIMENTAL TURBULENT BOUNDARY LAYER PROFILES

$M_\infty = 5.0$, $P_o = 4$ ATM, $T_o = 430°$ K

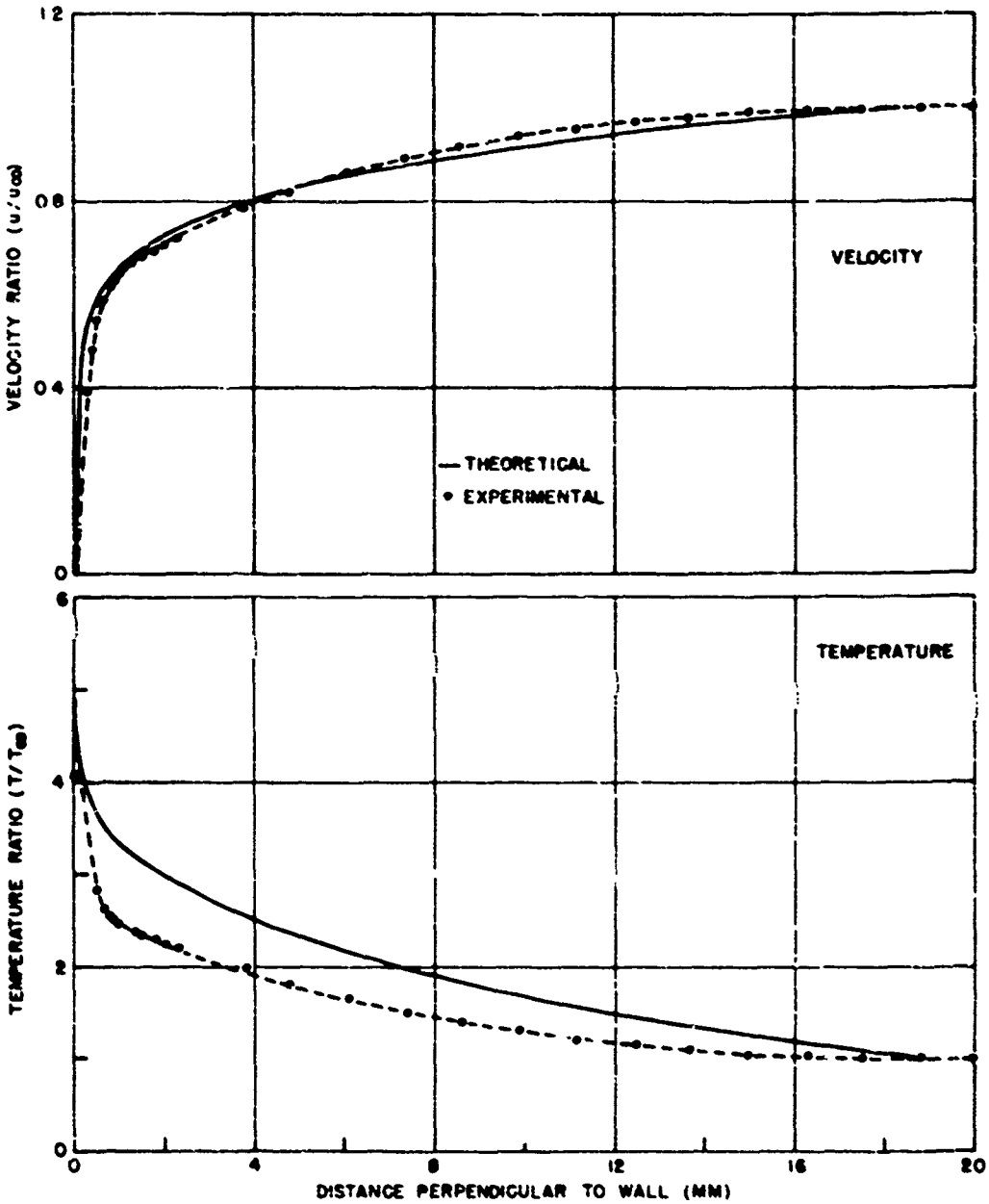

FIG. 9C COMPARISON BETWEEN THEORETICAL AND EXPERIMENTAL TURBULENT BOUNDARY LAYER PROFILES

$M_\infty = 5.0$, $P_o = 8$ ATM, $T_o = 430°K$

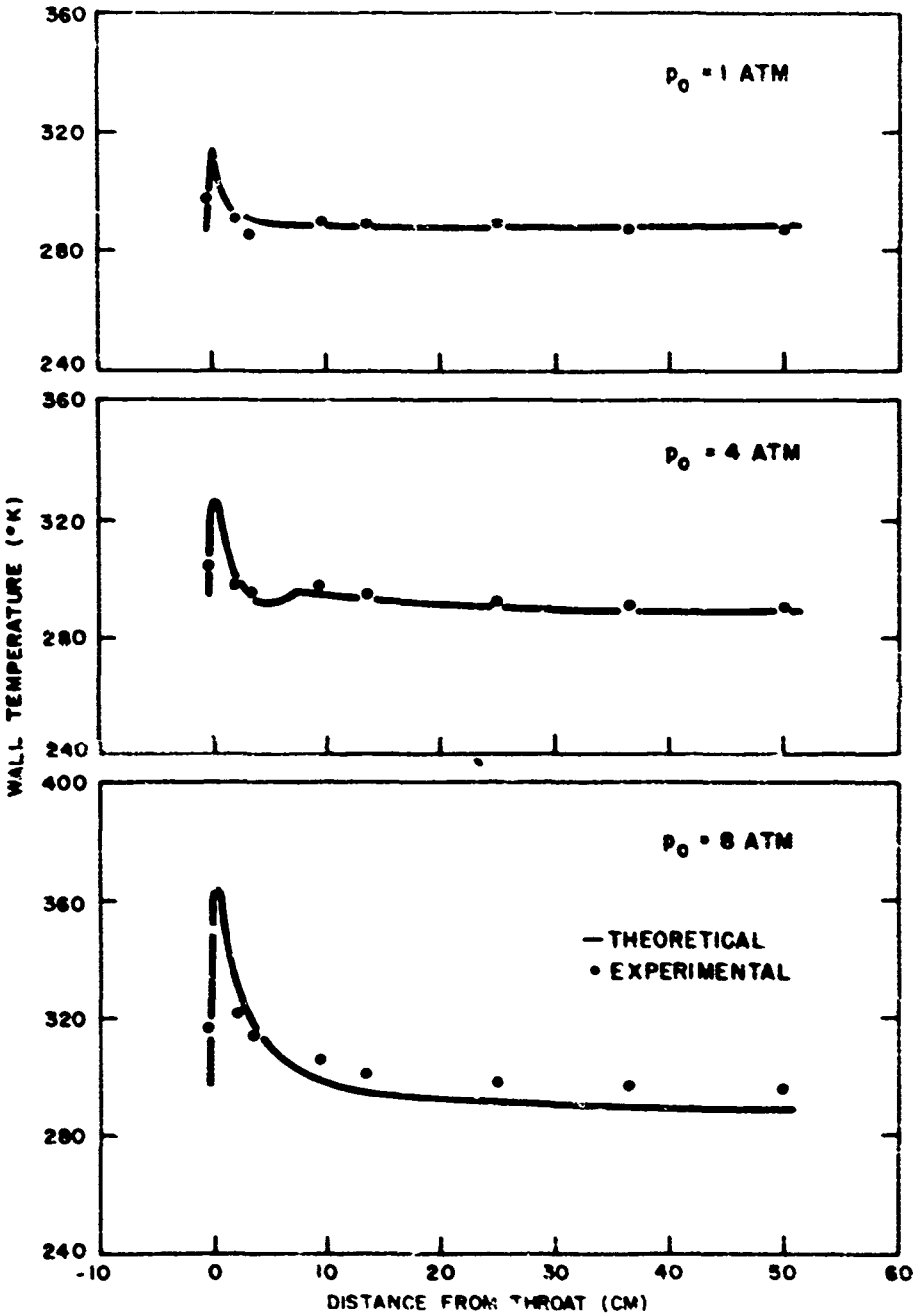

FIG 10 VARIATION OF THE WALL TEMPERATURE WITH AXIAL DISTANCE ALONG NOZZLE FOR THREE VALUES OF THE SUPPLY PRESSURE

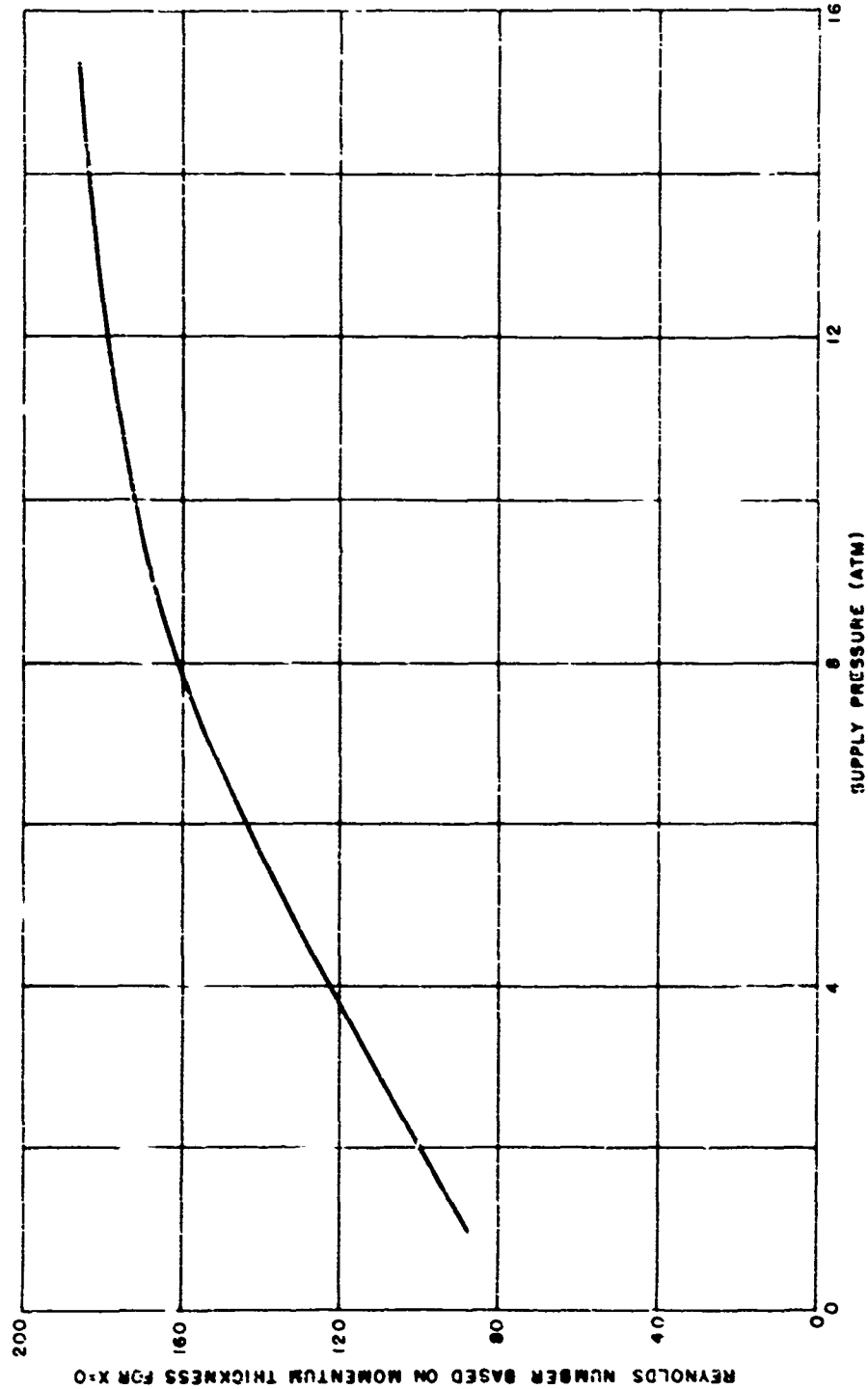

FIG. 11 VARIATION OF R_{e_θ} IN THROAT WITH SUPPLY PRESSURE

EXTERNAL DISTRIBUTION

No. of Copies	
1	Mr. A. I. Moskowitz Bureau of Ordnance (Re9a) Navy Department Washington, D. C.
1	Chief, Naval Operations Department of the Navy Washington 25, D. C.
2	The Artillery School Anti-aircraft & Guided Missiles Br. Fort Bliss, Texas Attn: Research & Analysis Sec.
1	Dr. K. F. Rubert Internal Aerodynamics Branch National Advisory Committee for Aeronautics Langley Field, Virginia
1	Prof. R. F. Probstein Division of Engineering Brown University Providence, Rhode Island
1	Commander U. S. Naval Proving Ground Dahlgren Virginia
1	Jet Propulsion Laboratory 4800 Oak Grove Drive Pasadena, California Attn: Dr. P. P. Wegener
1	Flight and Aerodynamics Laboratory Research Division Ordnance Missile Laboratory Redstone Arsenal Huntsville, Alabama Attn: J. L. Potter, Chief
5	U. S. Air Force Headquarters Arnold Engineering Development Center (ARDC) Tullahoma, Tennessee Attn: AEKS

No. of
Copies

1 Dr. R. H. Mills
Wright Air Development Center
Wright-Patterson Air Force Base
Dayton, Ohio

3 Mr. Ronald Smelt
Chief, Gas Dynamics Facility
Arnold Research Organization, Inc.
Tullahoma, Tennessee

1 Dr. Henry Nagamatsu
California Institute of Technology
Pasadena, California

1 Professor N. J. Hoff
Polytechnic Institute of Brooklyn
Brooklyn, New York

1 Dr. F. L. Wattendorf
Facilities Division DCS/Development
Hdqts. USAF, Room 5C368
Pentagon, Washington 25, D. C.

1 Professor A. Kantrowitz
Cornell University
Department of Aeronautical Engineering
Ithaca, New York

1 Professor Lester Lees
California Institute of Technology
Pasadena, California

1 Dr. H. G. Stever
MIT, Department of Aeronautical Engineering
Cambridge, Massachusetts

1 Professor G. L. Von Eschen
Aeronautical Engineering Department
Ohio State University
Columbus, Ohio

1 Mr. R. L. Bayless
Consolidated Vultee Aircraft Corporation
San Diego, California

1 Professor S. M. Bogdonoff
Department of Aeronautical Engineering
Princeton University
Princeton, New Jersey

No. of Copies	
1	Professor J. Kaye MIT, Physics Department Cambridge, Massachusetts
1	Professor Dean MIT, Gas Turbine Laboratory Engineering Department Cambridge, Massachusetts
1	Dr. Ruldolf Herman Department of Mechanical Engineering University of Minnesota Minneapolis 14, Minnesota
1	Dr. Ernst R. G. Eckert Department of Mechanical Engineering University of Minnesota Minneapolis 14, Minnesota
1	Mr. Mervin Sibulkin Jet Propulsion Laboratory 4800 Oak Grove Drive Pasadena, California
1	Dr. G. R. Eber Holloman Air Force Base Alamagordo, New Mexico
1	Dr. Albert E. Lombard Pentagon, Rm. 4E348 Washington, D. C.
1	Dr. A. Ferri Polytechnic Institute of Brooklyn 99 Livingston Street Brooklyn, New York
1	Dr. E. R. Van Driest Aerophysics Laboratory North American Aviation, Inc. Downing, California
1	Dr. Paul A. Libby Polytechnic Institute of Brooklyn 99 Livingston Street Brooklyn, New York

Aeroballistic Research Department
External Distribution List for Aeroballistics Research (XIa)

No of Copies

6 Office of Naval Research
Branch Office
Navy 100
Fleet Post Office
New York, New York

Commanding General
Aberdeen Proving Ground
Aberdeen, Maryland
1 Attn Dr B L Hicks

National Bureau of Standards
Aerodynamics Section
Washington 25, D C
1 Attn Dr G B Schubauer, Chief

Ames Aeronautical Laboratory
Moffett Field, California
1 Attn: Walter G Vincenti

University of California
Observatory 21
Berkeley 4, California
1 Attn: Leland E Cunningham
VIA: InsMat

Massachusetts Inst of Technology
Dept of Mathematics, Room 2-270
77 Massachusetts Avenue
Cambridge, Massachusetts
1 Attn: Prof Eric Reissner
VIA: InsMat

Graduate School Aeronautical Engr.
Cornell University
Ithaca, New York
1 Attn: W R Sears, Director
VIA: ONR

Applied Mech and Statistics Lab
Stanford University
Stanford, California
1 Attn R J Langle, Associate Dir
VIA: Ass't InsMat

University of Minnesota
Dept of Aeronautical Engr
Minneapolis, Minnesota
1 Attn: Professor R Hermann
VIA: Ass't InsMat

Case Institute of Technology
Dept of Mechanical Engineering
Cleveland, Ohio
1 Attn: Professor G Kuerti
VIA: ONR

Harvard University
109 Pierce Hall
Cambridge 38, Massachusetts
1 Attn: Professor R von Mises

Aeroballistic Research Department
External Distribution List for Aeroballistics Research (XI)

No. of Copies	
	Chief, Bureau of Ordnance Department of the Navy Washington 25, D C
1	Attn: Rea
1	Attn: Rexe
1	Attn: Re3d
2	Attn: Re6
3	Attn: Re9a
	Chief, Bureau of Aeronautics Department of the Navy Washington 25, D C
1	Attn: AER-TD-414
2	Attn: RS-7
	Commander U. S. Naval Ordnance Test Station Inyokern P O. China Lake, California
2	Attn: Technical Library
1	Attn: Code 5003
	Commander U S Naval Air Missile Test Center Point Mugu, California
2	Attn: Technical Library
	Superintendent U S Naval Postgraduate School Monterey, California
1	Attn: Librarian
	Commanding Officer and Director David Taylor Model Basin Washington 7, D C
2	Attn: Hydrodynamics Laboratory
	Chief of Naval Research Library of Congress Washington 25, D C
2	Attn: Technical Info Div
	Office of Naval Research Department of the Navy Washington 25, D C
1	Attn: Code 438
2	Attn: Code 463
	Director Naval Research Laboratory Washington 25, D C.
1	Attn: Code 2021
1	Attn: Code 3800
1	Officer-in-Charge Naval Aircraft Torpedo Unit U S Naval Air Station Quonset Point, Rhode Island
	Office, Chief of Ordnance Washington 25, D C
1	Attn: ORDTU

No of Copies	
2	Library Branch Research and Development Board Pentagon 3D104, Washington 25, D C
	Chief, AFSWP P O Box 2610 Washington 25, D C
1	Attn: Technical Library
1	Chief, Physical Vulnerability Branch Air Targets Division Directorate of Intelligence Headquarters, USAF Washington 25, D C
	Commanding General Wright Air Development Center Wright-Patterson Air Force Base Dayton, Ohio
5	Attn: WCAPD
1	Attn: WCSD
2	Attn: WCSOR
2	Attn: WCRRN
1	Attn: WCACD
1	Attn: WCRRF
1	Director Air University Library Maxwell Air Force Base, Alabama
	Commanding General Aberdeen Proving Ground Aberdeen, Maryland
1	Attn: C L Poor
1	Attn: D S Dederick
	National Bureau of Standards Washington 25, D C
1	Attn: Nat'l Applied Math Lab
1	Attn: Librarian (Ord Dev Div)
1	Attn: Chief, Mechanics Div
	National Bureau of Standards Corona Laboratories (Ord Dev Div) Corona, California
1	Attn: Dr H Thomas
	National Bureau of Standards Building 3U, UCLA Campus 405 Hilgard Avenue Los Angeles 24, California
1	Attn: Librarian
	University of California 211 Mechanics Building Berkeley 4, California
1	Attn: Dr R G Folsom
1	Attn: Mr G Maslach
1	Attn: Dr S A Schaaf VIA: InsMat

Aeroballistic Research Department
External Distribution List for Aerobaillstics Research (XI)

No of Copies	
	Chief, Bureau of Ordnance Department of the Navy Washington 25, D C
1	Attn: Rea
1	Attn: Rexe
1	Attn: Re3d
2	Attn: Re6
3	Attn: Re9a
	Chief, Bureau of Aeronautics Department of the Navy Washington 25, D C
1	Attn: AER-TD-414
2	Attn: RS-7
	Commander U. S. Naval Ordnance Test Station Inyokern P O China Lake, California
2	Attn: Technical Library
1	Attn: Code 5003
	Commander U S Naval Air Missile Test Center Point Mugu, California
2	Attn: Technical Library
	Superintendent U S Naval Postgraduate School Monterey, California
1	Attn: Librarian
	Commanding Officer and Director David Taylor Model Basin Washington 7, D C
2	Attn: Hydrodynamics Laboratory
	Chief of Naval Research Library of Congress Washington 25, D C
2	Attn: Technical Info Div
	Office of Naval Research Department of the Navy Washington 25, D C
1	Attn: Code 438
2	Attn: Code 463
	Director Naval Research Laboratory Washington 25, D C
1	Attn: Code 2021
1	Attn: Code 3800
1	Officer-in-Charge Naval Aircraft Torpedo Unit U S Naval Air Station Quonset Point, Rhode Island
	Office, Chief of Ordnance Washington 25, D. C
1	Attn: ORDTU

No of Copies	
2	Library Branch Research and Development Board Pentagon 3D104, Washington 25, D C
	Chief, AFSWP P O. Box 2610 Washington 25, D C
1	Attn: Technical Library
1	Chief, Physical Vulnerability Branch Air Targets Division Directorate of Intelligence Headquarters, USAF Washington 25, D C
	Commanding General Wright Air Development Center Wright-Patterson Air Force Base Dayton, Ohio
5	Attn: WCAPD
1	Attn: WCSD
2	Attn WCSOR
2	Attn: WCRRN
1	Attn: WCACD
1	Attn: WCRRF
1	Director Air University Library Maxwell Air Force Base, Alabama
	Commanding General Aberdeen Proving Ground Aberdeen, Maryland
1	Attn: C L Poor
1	Attn: D S Dederick
	National Bureau of Standards Washington 25, D C
1	Attn: Nat'l Applied Math Lab
1	Attn: Librarian (Ord Dev Div)
1	Attn: Chief, Mechanics Div '
	National Bureau of Standards Corona Laboratories (Ord Dev Div) Corona, California
1	Attn: Dr H Thomas
	National Bureau of Standards Building 3U, UCLA Campus 405 Hilgard Avenue Los Angeles 24, California
1	Attn: Librarian
	University of California 211 Mechanics Building Berkeley 4, California
1	Attn: Dr R G. Folsom
1	Attn: Mr G ' Maslach
1	Attn: Dr S A Schaaf VIA: InsMat

No. of
Copies

North American Aviation, Inc.
12214 Lakewood Boulevard
Downey, California
2 Attn: Aerophysics Library
VIA: BuAero Representative

United Aircraft Corporation
East Hartford 8, Connecticut
1 Attn: Robert C. Sale
VIA: BuAero Representative

National Advisory Committee for Aero
1724 F Street, Northwest
Washington 25, D. C.
5 Attn: E. B. Jackson

Ames Aeronautical Laboratory
Moffett Field, California
1 Attn: H.J. Allen
2 Attn: Dr. A.C. Charters

NACA Lewis Flight Propulsion Lab.
Cleveland Hopkins Airport
Cleveland 11, Ohio
1 Attn: John C. Evvard

Langley Aeronautical Laboratory
Langley Field, Virginia
1 Attn: Theoretical Aerodynamics Div.
1 Attn: J. V Becker
1 Attn: Dr. Adolf Busemann
1 Attn: Mr. C H. McLellan
1 Attn: Mr. J Stack

Harvard University
21 Vanserg Building
Cambridge 38, Massachusetts
1 Attn: Prof. Garrett Birkhoff

The Johns Hopkins University
Charles and 34th Streets
Baltimore 18, Maryland
1 Attn: Dr. [illegible] Clauser

New York University
45 Fourth Avenue
New York 3, New York
1 Attn: Professor R Courant

1 Dr. Allen E. Puckett, Head
Missile Aerodynamics Department
Hughes Aircraft Company
Culver City, California

1 Dr Gordon N. Patterson, Director
Institute of Aerophysics
University of Toronto
Toronto 5, Ontario, Canada
VIA: BuOrd (Ad8)